The effect of atomic force microscope probe size on indentation tests simulated using realistic surface forces

Michael A. Graham, Zachary C. Grasley and Rashid K. Abu Al-Rub*

Zachry Department of Civil Engineering,
Texas A&M University,
710B CE/TTI, 3136 TAMU,
College Station, TX 77843-3136, USA
Fax: 979-845-6554
E-mail: mikegraham@gmail.com
E-mail: zgrasley@civil.tamu.edu
E-mail: rabualrub@civil.tamu.edu
*Corresponding author

Abstract: The effects of the size and shape of an indenter tip used in a nanoscale indentation test (such as with an atomic force microscope) are studied using realistic, finite-range surface forces to describe the contact and extended-range interaction of the indenter and sample. Sphero-conical indenters with tips ranging from sharp-pointed to very rounded tips (similar to spherical tips) are studied. A continuum Lennard-Jones adhesion potential and a Poisson-Boltzmann exponential repulsion law are used to study adhesive and repulsive-only interactions, respectively. The size of the tip affects the qualitative response for an adhesive surface force potential, with increasingly rounded tips exhibiting a more pronounced jump into contact and a greater overall adhesion. The effects of tip size are less pronounced for pure repulsion.

Keywords: atomic force microscopy; size effect; nanoindentation; surface forces; non-local effects; adhesive force; contact force.

Reference to this paper should be made as follows: Graham, M.A., Grasley, Z.C. and Abu Al-Rub, R.K. (2010) 'The effect of atomic force microscope probe size on indentation tests simulated using realistic surface forces', *Int. J. Materials and Structural Integrity*, Vol. 4, Nos. 2/3/4, pp.160–169.

Biographical notes: Michael Graham is a PhD student in the Zachry Department of Civil Engineering at Texas A&M University (TAMU). He obtained his BS and MS in Civil Engineering from TAMU. His research interests are in computational mechanics and constitutive modelling of the inelastic behaviour of materials at the several length and time scales.

Zachary C. Grasley is an Assistant Professor in the Materials Division of the Zachry Department of Civil Engineering at Texas A&M University. He received his BS in Civil Engineering from Michigan Technological University, and his MS and PhD in Civil Engineering from the University of Illinois, Urbana-Champaign. He is a member of ACI Committees 231, Properties of Concrete at Early Ages and 236, Material Science of Concrete. His research interests include internal relative humidity, poromechanics, durability,

viscoelasticity of concrete and novel cementitious materials.

Rashid K. Abu Al-Rub is an Assistant Professor of Civil Engineering at Texas A&M University. He received his BS and MS in Civil Engineering from Jordan University of Science & Technology and his PhD in Civil Engineering from Louisiana State University. His research interests include computational solid mechanics, size-scale effects, nanocomposites and constitutive modelling of the inelastic, damage and fracture behavior of a wide range of engineering materials.

1 Introduction

To study the mechanical properties of materials at the nanoscale, researchers conduct tests using atomic force microscopy (AFM), wherein a very small probe interrogates the surface of a sample for imaging or testing. One mechanical test utilising AFM is indentation, a test where the probe is pressed into the sample and the force is measured. The tips of AFM probes vary greatly in size, shape and material, but traditional analysis methods only consider extremely simple geometries (Hertz, 1881; Johnson et al., 1971; Derjaguin et al., 1975; Barber and Billings, 1990; Bilodeau, 1992).

Further, the forces which drive the deformation, most notably van der Waals attraction and electric double layer repulsion, have finite range and have been detected at separations up to about 100 nm (Israelachvili, 1991). Though there has been some study of different shapes for indenters in nanoscale tests (Barber and Billings, 1990; Bilodeau, 1992; Fischer-Cripps, 2000), *all* classical contact models only consider infinitesimal-range forces (Hertz, 1881; Johnson et al., 1971; Derjaguin et al., 1975). Though it is reasonable to neglect the extended range of the fundamental surface forces at large scales, at the scale of AFM indentation tests, the extended range of the forces may be important.

Attard and Parker (1992) and Attard (2000) considered the interaction of bodies due to their finite-range interaction forces, but their studies were limited to spherical bodies (i.e., the shape of the contact surfaces was fully characterised by an effective radius). No past studies have used finite range surface forces for indenters of other shapes, so this study analyses various sphero-concical tips which undergo deformation due to realistic, finite-range surface forces.

2 Finite-range interaction model

2.1 Kinematic definitions

Consider two bodies being pushed together, as in an indentation test. The *separation* $h(\boldsymbol{r})$ is the distance between points on the two bodies' surfaces measured parallel to the axis of the forced motion at a point $\boldsymbol{r}$ in the plane perpendicular to the axis of motion. The *undeformed separation* $h_0(\boldsymbol{r})$ is the separation at $\boldsymbol{r}$ which would occur if no deformation occurred. The undeformed separation will be negative $h_0(\boldsymbol{r}) < 0$ if the bodies would have interpenetrated had no deformation had occurred. The undeformed

separation is rigid: it can be calculated from a single point – this study will use the *position* $h_0^\star$ –and a function describing the undeformed shapes of the interacting bodies which is the same for all configurations[1]. That is,

$$h_0(\boldsymbol{r}) = h_0^\star + C(\boldsymbol{r}), \tag{1}$$

where $h_0^\star$ varies through a simulation or test and $C(r)$ remains constant, but is different for various probe shapes. The *deformation* $u(\boldsymbol{r})$ is the average displacement of the two bodies' surfaces from their undeformed shapes parallel to the axis of forced motion at point $\boldsymbol{r}$, defined so that extensions (the bodies bulging toward each other) are positive.

The separation $h(\boldsymbol{r})$, undeformed separation $h_0(\boldsymbol{r})$, and deformation $u(\boldsymbol{r})$ satisfy

$$h(\boldsymbol{r}) = h_0(\boldsymbol{r}) - 2u(\boldsymbol{r}). \tag{2}$$

The undeformed separation $h_0(\boldsymbol{r})$ is known for a displacement-driven simulation (or test), and $u(\boldsymbol{r})$ or $h(\boldsymbol{r})$ is the solution variable.

Figure 1 illustrates the separation $h(\boldsymbol{r})$, undeformed separation $h_0(\boldsymbol{r})$, and deformation $u(\boldsymbol{r})$. The two bodies are depicted as bulging toward each other. Note that u is the *average* deformation of the bodies, and that it is positive for attraction.

Figure 1 Diagram illustrating the separation h, undeformed separation h_0, and deformation u for two arbitrarily-shaped bodies (see online version for colours)

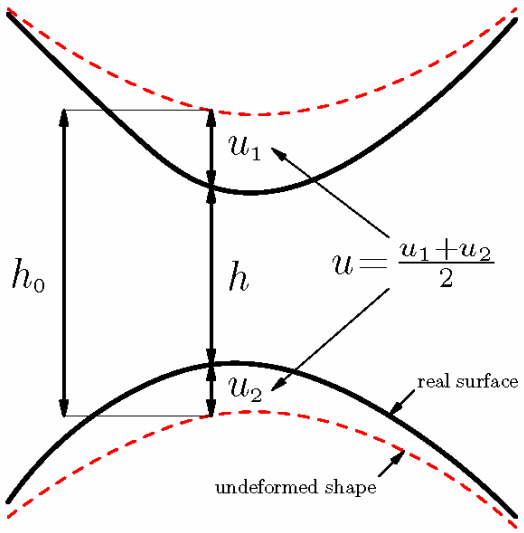

2.2 *Model formulation*

The deformation u of a semi-infinite, isotropic, elastic body due to a pressure field $p_r(\boldsymbol{r})$ is (Landau and Lifshitz, 1970; Attard, 2000)

$$u(\boldsymbol{r}) = -\frac{2}{\pi E_{\text{eff}}} \int_\Omega \frac{p_r(\boldsymbol{s})}{|\boldsymbol{r} - \boldsymbol{s}|} d\boldsymbol{s}, \tag{3}$$

where E_{eff} is a measure of the elastic properties of the bodies such that

$$\frac{2}{E_{\text{eff}}} = \frac{1-\nu_1^2}{E_1} + \frac{1-\nu_2^2}{E_2}, \tag{4}$$

where $E_1, \nu_1, E_2,$ and ν_2 are the Young's moduli and Poisson's ratios for the two bodies 1 and 2. The domain of integration Ω is the whole plane perpendicular to the direction of motion. This expression describes a flat, semi-infinite elastic body, but elasticity solutions for not exist for the shapes used in practice. All classical contact models make major assumptions regarding the deformation of contacting bodies (Hertz, 1881; Johnson et al., 1971; Derjaguin et al., 1975), and the results due to this approximation presented in this paper conform to physical expectations.

The mutual interaction (related to the distance between the surfaces) drives the deformation, so the this dependence is included by setting the pressure to be a function of the separation $p_r(\boldsymbol{r}) = p(h(\boldsymbol{r}))$. Equation (3) becomes

$$u(\boldsymbol{r}) = -\frac{2}{\pi E_{\text{eff}}} \int_{\Omega} \frac{p(h(\boldsymbol{s}))}{|\boldsymbol{r}-\boldsymbol{s}|} d\boldsymbol{s}, \tag{5}$$

which gives the deformation at each point $\boldsymbol{r}$ as a function of the pressure, which is in turn a function of the separation h [recall (2)]; a method for solving this implicit equation is presented by Attard and Parker (1992) and Attard (2000).

Equation (5) may be used as-is, but much computational expense can be saved by applying axisymmetry. In this case, the deformation is calculated by

$$u(r) = -\frac{2}{E_{\text{eff}}} \int_0^{\infty} p(h(s))\, k(r,s) s ds, \tag{6}$$

where the kernel is

$$k(r,s) = \begin{cases} \frac{4}{\pi r} K\left(s^2/r^2\right) & s < r \\ \frac{4}{\pi r} K\left(r^2/s^2\right) & s > r \end{cases}, \tag{7}$$

where $K(m)$ is the complete elliptic integral of the first kind. The derivation of the axisymmetric form is presented in Appendix. A workaround for the singularity at $K(1)$ is provided by Attard (2000).

The total force can be calculated by integrating the pressure:

$$F = \int_{\Omega} p(\boldsymbol{r})\, d\boldsymbol{r} = 2\pi \int_0^{\infty} p(r)\, r dr. \tag{8}$$

2.3 Surface forces

Many surface pressures have been proposed for studying electric double layer repulsion and van der Waals attraction, and some can be adapted for solving the continuum problem. This paper addresses cases of pure repulsion and repulsion with adhesion. The potentials used for the two cases are a Lennard-Jones adhesion

$$p(h) = \frac{A}{6\pi h^3}\left[\left(\frac{z_0}{h}\right)^6 - 1\right] \tag{9}$$

with Hamaker constant A and equilibrium separation z_0 for the repulsive-adhesive case and a Poisson-Boltzmann repulsion

$$p(h) = P_0 \exp(-\kappa h), \tag{10}$$

with material constants P_0 and κ governing the magnitude and range of the pressure, respectively, for the repulsive-only case. These surface pressures are chosen to match those used in previous studies of finite-range interaction (Attard and Parker, 1992; Attard, 2000).

3 Tip shape effects

3.1 Computational regimen

Five tip shapes are considered, all of which are based on a right circular cone subtended by angle θ with a spherical end of radius r_t. The shape is represented piecewise using the equations for a circle and a line, and the regions meet when the slope of the circle is equal to the slope of the line. Figure 2 shows the shape of the probe, and the sample is initially flat in all cases.

Figure 2 Tip shape is defined by the inner angle θ and the radius of the rounded end r_t (see online version for colours)

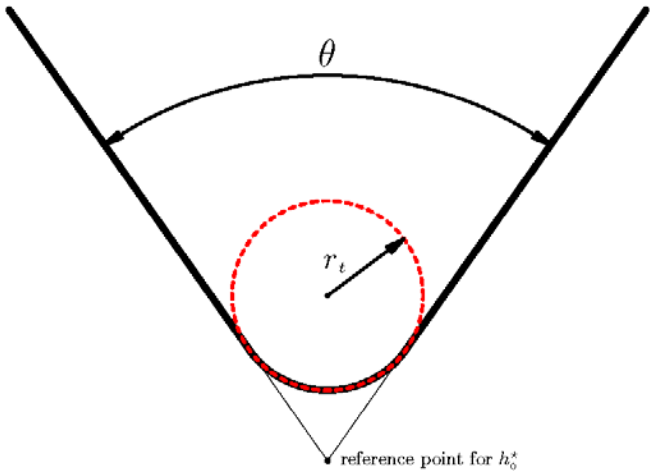

Simulations were conducted for $r_t = 0$ (a sharp-tipped cone) and $r = 1, 2, 4,$ and 6 nm, with $\theta = 60°$ in all cases. (AFM tips with tip end radii at least as small as 2 nm are readily commercially available). The position $h_0^\star$ is defined as the distance between the tip and the sample at $r = 0$ *if the tip was a sharp-tipped cone*, and it varies from 5 nm to –5 nm in 0.05 nm steps.

For repulsive-adhesive simulations, the Lennard-Jones adhesion potential given in (9) was used, with Hamaker constant $A = 10^{-14}$ J, equilibrium separation $z_0 = 1$ nm, and effective stiffness $E_{\text{eff}} = 1$ GPa.

For repulsive-only simulations, the Poisson-Boltzmann type law given in (10) is used, with amplitude $P = 10,000$ GPa, range parameter $\kappa = 1$ nm, and effective stiffness $E_{\text{eff}} = 250$ GPa.

3.2 Results

Figure 3 shows the separations at various positions for the sharp-tipped cone ($r_t = 0$ nm) and the cone with tip end radius $r_t = 2$ nm for adhesive behaviour. In the pre-contact and early contact region, the differences due to the shape of the tip are clear, but as the bodies move closer together, the effects of the probe end shape vanish.

Figure 4 shows the separations at various separations for the cone with tip end radius $r_t = 4$ nm for adhesive behaviour. The shapes are very similar, except that the jump occurs at a closer separation in loading than unloading. This matches physical expectations, but is not consistent with the elastic formulation used for the model and is postulated to be a numerical artefact.

Figure 5 is a plot of the total force F versus the position $h_0^\star$ for various tip shapes for the adhesive case. As the shapes become more rounded, the jump becomes more pronounced. As the bodies move closer together after the jump, the responses become more qualitatively similar. The maximum negative force is larger for bodies with increasingly rounded ends, i.e. they exhibit more adhesion.

Figure 6 is a plot of the total force F versus the position $h_0^\star$ for various tip shapes for the purely repulsive case. For this case, the effect of the shape contributes less noticeably to the qualitative behaviour observed. Notice that as the bodies move closer together, the plots become more alike.

Figure 3 The separation $h(r)$ due to the Lennard-Jones adhesive law at positions $h_0^\star = 3,1,-1,-3,-5$ nm (loading) for the sharp-tipped cone ($\theta = 60°, r_t = 0$) (right) and the cone with $r_t = 2$ nm (left) (see online version for colours)

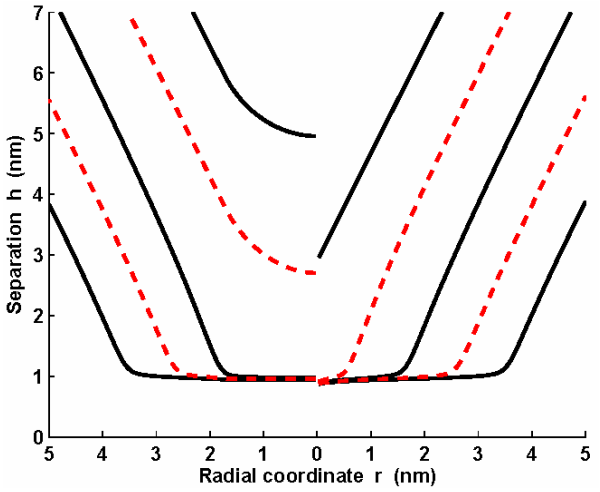

Figure 4 Separation $h(r)$ due to the Lennard-Jones adhesive law at positions $h_0^\star = 3, 1, -1, -3, -5$ nm for loading (right) and unloading (left), for the round-tipped with tip radius $r_t = 4$ nm (see online version for colours)

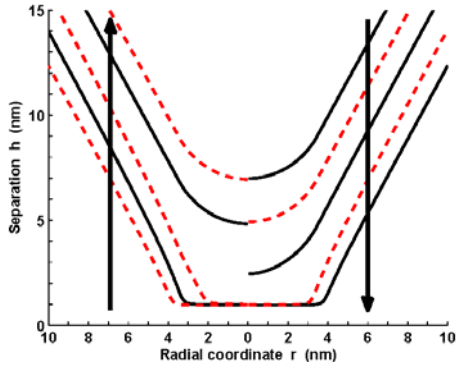

Figure 5 Total force F vs. position $h_0^\star$ for loading for various indenter shapes, for the Lennard-Jones adhesion surface force law (see online version for colours)

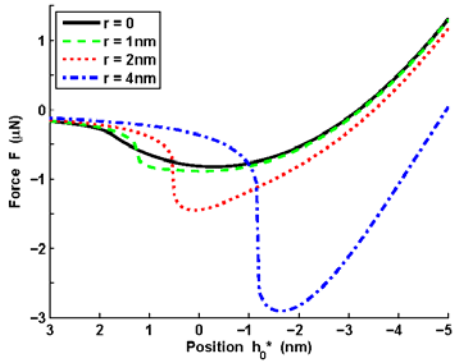

Figure 6 Total force F vs. position $h_0^\star$ for loading for all indenter shapes, for the Poisson-Boltzmann repulsion surface force law (see online version for colours)

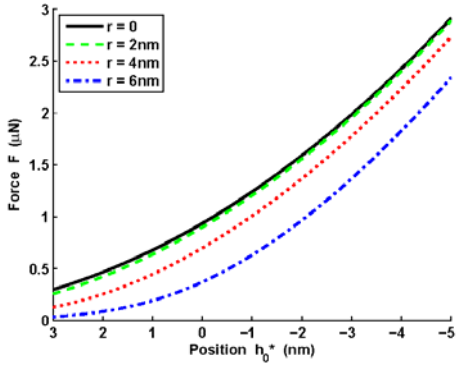

4 Conclusions

4.1 Findings

Tip geometry greatly affects the qualitative and quantitative results of an indentation test. Small changes in tip geometry do not appear to effect major changes in overall behaviour; that is, the response appears to be stable with respect to tip size and shape. For adhesion, the effects are very significant, with a more pronounced jump into contact and greater adhesion for rounded tips. There is less qualitative difference in the response for pure repulsion, but tip shape has a definite effect. In an AFM indentation test designed to determine a property like stiffness or surface energy, researchers should be especially aware of tip shape effects when testing very compliant, adhesive materials.

4.2 Future work

The method for solving finite-range interaction problems used in this paper is extremely robust and can be solved to study many problems. Several tip shapes are considered here, but others exist, most notably pyramidal tips, which are not axisymmetric and would require a modified numerical implementation, but the main governing equation (5) can be used for non-axisymmetric tips.

Attard (2001) studied the response of linear viscoelastic solids due to finite-range surface forces, but only for spherical geometries. To study the effect of tip shape in AFM indentation tests involving viscoelastic particles, a similar study to the one presented here will use viscoelastic material behaviour. Other material laws may be explored, but (3) is specifically developed for elastic materials [and can be extended to linear viscoelastic materials using the correspondence principle, as by Attard (2001)].

Some very small interactions between bodies have been studied using molecular dynamics. The continuum model presented and used in this paper should be used to model the same processes modelled using molecular dynamics to test its strengths.

Acknowledgements

The authors gratefully acknowledge the financial support provided by the Southwest University Transportation Center and the assistance of Dr. Phil Attard of the University of Sydney.

References

Abramowitz, M. and Stegun, I.A. (1972) *Handbook of Mathematical Functions with Formulas, Graphs, and Mathematical Tables*, US Department of Commerce.

Attard, P. (2000) 'The interaction and deformation of elastic bodies the origin of adhesion hysteresis', *Journal of Physical Chemistry*, Vol. 104, pp.10635–10641.

Attard P. (2001) 'Interaction and deformation of viscoelastic particles: nonadhesive particles', *Physical Review E*, Vol. 63, pp.061601-1–061604-9.

Attard, P. and Parker, J.L. (1992) 'Deformation and adhesion of elastic bodies in contact', *Physical Review A*, December, Vol. 46, No. 12, pp.7959–7971.

Barber, J.R. and Billings, D.A. (1990) *An Approximate Solution for the Contact Area and Elastic Compliance of a Smooth Punch of Arbitrary Shape*, Vol. 32, No. 12, pp.991–997.

Bilodeau, G.G. (1992) 'Regular pyramid punch problem', *Journal of Applied Mechanics*, Vol. 59, No. 3, pp.519–523, doi: 10.1115/1.2893754.

Derjaguin, B.V., Muller, V.M. and Toporov, Y.P. (1975) 'Effect of contact deformations on the adhesion of particles', *Journal of Colloid and Interface Science*, Vol. 53, No. 2, pp.314–326.

Fischer-Cripps, A.C. (2000) *Introduction to Contact Mechanics*, Springer.

Hertz, H. (1881) 'Ueber die Berührung fester elastischer Körper (On the contact of elastic solids)', *Journal Reine und Angewandte Mathematik*, Vol. 92, pp.156–171.

Israelachvili, J.N. (1991) *Intermolecular and Surface Forces*, 2nd ed., Academic Press.

Johnson, K.L., Kendall, K. and Roberts, A.D. (1971) 'Surface energy and contact of elastic solids', *Proceedings of the Royal Society of London*, Vol. 324, No. 1558, pp.301–313.

Landau, L.D. and Lifshitz, E.M. (1970) *Theory of Elasticity*, Pergamon.

Notes

1 It may be possible for the 'undeformed shape' to change during interaction due to an unrelated phenomenon, such as thermal dilation, but such cases will not be discussed in this paper.

Appendix

Derivation of the axisymmetric governing equation

To arrive at the axisymmetric form given in (A.8), consider the general form of the deformation due to a pressure

$$u(\boldsymbol{r}) = -\frac{2}{\pi E_{\text{eff}}}\int_{\Omega}\frac{p(h(\boldsymbol{s}))}{|\,\boldsymbol{r}-\boldsymbol{s}\,|}ds, \tag{A.1}$$

and substitute polar coordinates $\boldsymbol{r} = \langle r, \beta \rangle$ so that

$$u(r,\beta) = \frac{-2}{\pi E_{\text{eff}}}\int_0^{\infty}\int_0^{2\pi}\frac{p(h(s,\beta))}{\left|\langle r,\beta\rangle - \langle s,\phi\rangle\right|}s\,d\phi\,ds, \tag{A.2}$$

and recognise that the axisymmetric condition requires that functions do not vary with β (or the dummy variable corresponding to it, ϕ). Eliminating dependence on β and rearranging yields

$$\begin{aligned} u(r) &= \frac{-2}{E_{\text{eff}}}\int_0^{\infty}p(h(s))\left(\frac{1}{\pi}\int_0^{2\pi}\frac{d\phi}{\left|\langle r,0\rangle - \langle s,\phi\rangle\right|}\right)sds \\ &= \frac{-2}{E_{\text{eff}}}\int_0^{\infty}p(h(s))k(r,s)sds. \end{aligned} \tag{A.3}$$

The denominator of the integral in $k(r,s)$ is the distance between the tips of two vectors of length r and s subtended by angle ϕ. Assume $r > s$, then from trigonometry

$$\left|\langle r,0\rangle - \langle s,\phi\rangle\right| = \sqrt{r^2 - (s\sin\phi)^2}. \tag{A.4}$$

Rearranging,

$$\left|\langle r,0\rangle - \langle s,\phi\rangle\right| = r\sqrt{1-\frac{s^2}{r^2}\sin^2\phi}, \tag{A.5}$$

and substituting into $k(r,s)$ from (A.3),

$$k(r,s) = \frac{1}{\pi r}\int_0^{2\pi} \frac{d\phi}{\sqrt{1-\frac{s^2}{r^2}\sin^2\phi}}. \tag{A.6}$$

Recognising the periodicity of $\sin^2\phi$,

$$k(r,s) = \frac{4}{\pi r}\int_0^{\pi/2} \frac{d\phi}{\sqrt{1-\frac{s^2}{r^2}\sin^2\phi}}. \tag{A.7}$$

This integral is the complete elliptic integral of the first kind $k(m = s^2/r^2)$ (Abramowitz and Stegun, 1972). Substituting, (A.3) becomes

$$u(r) = -\frac{2}{E_{\text{eff}}}\int_0^{\infty} p(h(s))k(r,s)\,s\,ds, \tag{A.8}$$

where

$$k(r,s) = \frac{4}{\pi r}K\left(s^2/r^2\right). \tag{A.9}$$

Making the opposite assumption $s > r$, we can follow the same exact process starting at (A.4) to find

$$k(r,s) = \begin{cases} \frac{4}{\pi r}K\left(s^2/r^2\right) & s < r \\ \frac{4}{\pi r}K\left(r^2/s^2\right) & s > r \end{cases}. \tag{A.10}$$